Journal of Rare Cardiovascular Diseases

ISSN: 2299-3711 (Print) | e-ISSN: 2300-5505 (Online) www.jrcd.eu



RESEARCH ARTICLE

Synergistic Effect of Panax Ginseng-Mediated FeO Nanoparticles on Colon Cancer Cell (HT-29) Growth Inhibition

Balaji MB¹, Thomas N², Shalin Prakash¹ and Vimal S^{1*}

¹Department of Biochemistry, Saveetha Medical College and Hospitals, Saveetha Institute of Medical and Technical Sciences, Saveetha University, Chennai, Tamil Nadu, India.

²Department of General Medicine, Saveetha Medical College and Hospitals, Saveetha Institute of Medical and Technical Sciences, Saveetha University, Chennai, Tamil Nadu, India.

*Corresponding Author Vimal S

Article History
Received: 09/07/2025
Revised: 23/08/2025
Accepted: 12/09/2025
Published: 30/09/2025

Abstract: Nanoparticles generated utilizing plant-mediated methods have attracted substantial interest in biomedical applications owing to their biocompatibility and increased therapeutic effectiveness. In this work, iron oxide nanoparticles (P-FeO) were synthesized using Panax ginseng extract as a natural reducing and capping source. Structural confirmation through FTIR spectroscopy identified key functional signals for hydroxyl, aromatic, sulfonyl, and alkene bonds, verifying the surface attachment of P. ginseng metabolites that enhance particle stability and interaction with biological targets. SEM imaging displayed well-defined, pentagonal nanoparticles with uniform dispersion, indicating that phytochemicals guided the nucleation and growth process. When tested on HT-29 colon cancer cells, the P-FeO nanoparticles exhibited notable cytotoxicity with an IC₅₀ value of 8.7 μg/mL. Morphological observation and fluorescence microscopy revealed apoptosis characterized by cell shrinkage, blebbing, and nuclear fragmentation. The mechanism is likely linked to ROS overproduction, mitochondrial depolarization, and activation of caspase-3 and Bax, along with suppression of Bcl-2, confirming a mitochondrial-driven apoptotic route. Antioxidant and antiinflammatory tests showed concentration-dependent inhibition of free radicals and cytokines such as TNF- α and IL-6, aligning with reduced oxidative stress and inflammatory signaling. The nanoparticles also demonstrated a biphasic drug-release profile, achieving full release within 24 hours, suggesting efficient therapeutic delivery. Collectively, the findings indicate that Panax ginseng-functionalized FeO nanoparticles exert anticancer effects through ROS-mediated apoptosis and inflammatory marker modulation, offering a biocompatible and effective approach for colon cancer treatment.

Keywords: Iron oxide nanoparticles (FeO NPs), colon cancer, HT-29 cells, cytotoxicity, MTT assay, apoptosis, fluorescence microscopy.

INTRODUCTION

A complex disorder, cancer is defined by the uncontrolled proliferation of cells that can spread to other regions of the body. This abnormal cell growth has the capacity to invade surrounding tissues and organs. These diseases have been among the most significant causes of death, mainly because of their complexity and the difficulties in halting their spread. According to the GLOBOCAN estimates of 2020 [1], cancer remains a major health concern globally. This impact is expected to grow due to factors like population aging and growth, especially in developing nations, which comprise approximately 82% of the world's population. In less economically developed regions, Behavioral patterns including tobacco use, poor nutrition, sedentary habits, and changes in reproductive health (e.g., delayed childbirth and lower parity) are increasingly contributing to the rising cancer burden [2]. This trend underscores the role of environmental carcinogens and mutagens in the initiation of cancer [3]. Preventive strategies aim to lower cancer incidence and associated mortality by addressing these risk factors. Cells form the basic structural and functional units of body tissues, governed by genes that regulate growth, repair, and programmed cell death. When genetic mutations disrupt these controls, cells can proliferate excessively and avoid normal death processes, leading to the formation of

masses, or tumors. Neoplasms can be categorized into two distinctive types: non-cancerous (benign) and cancerous (malignant). Malignant neoplasms have the ability to infiltrate nearby tissues and shift to other internal areas, a phenomenon called metastasis [4]. Green chemistry approaches, especially plant-mediated methods, have gained popularity as an economical and environmentally acceptable substitute for conventional chemical and physical synthesis methods in the production of FeO NPs. The anticancer, antiinflammatory, and antioxidant qualities of the wellknown medicinal plant Panax ginseng have been the subject of much research [5]. In addition to adding to Panax ginseng's medicinal effectiveness, its bioactive components ginsenosides, polysaccharides, flavonoids also work well as stabilizing and reducing agents during the nanoparticle production process [6]. Because of the synergistic interaction between the nanomaterial and the bioactive chemicals, combining Panax ginseng extracts with FeO NPs may increase the therapeutic effectiveness of the nanoparticles while reducing side effects. This study's justification is the mounting evidence that plant-mediated nanoparticles are more biocompatible and have anticancer properties than their chemically manufactured counterparts [7]. For example, prior research has shown that greensynthesized FeO NPs had strong cytotoxic effects on a range of cancer cell lines, such as liver, lung, and breast



cancer, while preserving healthy cells [8]. However, nothing is known about how well Panax ginsengmediated FeO NPs can target colon cancer cells, especially HT-29. Because of their fast proliferation and resistance to traditional treatments, HT-29 cells a wellestablished model for human colon adenocarcinoma are a perfect fit for testing new anticancer drugs [9]. The purpose of this work is to examine how Panax ginsengmediated FeO NPs may work in concert to limit the proliferation of HT-29 colon cancer cells. We predict that the bioactive substances in Panax ginseng will enhance the anticancer effects of FeO NPs, causing HT-29 cells to become more cytotoxic, induce apoptosis, and undergo cell cycle arrest. We created FeO NPs using Panax ginseng extract in order to verify this theory, and we used cutting-edge methods including their physicochemical qualities were evaluated utilizing modern methods to investigate structural. morphological, and compositional aspects. The MTT test was used to assess the nanoparticles harmful effects, and flow cytometry was implemented to evaluate the cell cycle and apoptosis. To further understand the underlying molecular processes, the replication of major apoptotic markers, including caspase-3 and Bcl-2, was examined. The results of this investigation may provide important new information on the possibility of Panax ginseng-mediated FeO NPs as a colon cancer treatment. This strategy may open the door to the creation of safer and more effective cancer treatments by using the complementary relationship between nanotechnology and plant bioactive chemicals. Additionally, the environmentally friendly synthesis approach supports sustainable and ecologically conscious scientific activities by being consistent with the ideas of green chemistry. Innovative approaches like these are desperately required to enhance patient outcomes and lessen the socioeconomic effect of this debilitating illness as the worldwide incidence of colon cancer keeps increasing.

METHODOLOGY

2.1 Preparation of Panax ginseng FeO Nps

The preparation of Panax ginseng-mediated iron oxide nanoparticles involved several interconnected steps, where the plant extract acted simultaneously as a stabilizer and reducing agent. Fresh P. ginseng roots (20 g) were rinsed thoroughly with distilled water, cut into small slices, and boiled in 200 mL of distilled water for 30 minutes at 70 °C. The mixture was cooled to room temperature and filtered through Whatman No. 1 paper to obtain a clear aqueous extract. For nanoparticle synthesis, 50 mL of the extract was added dropwise to 100 mL of 0.1 M ferric chloride (FeCl₃) solution under constant magnetic stirring at 60 °C. A gradual shift in color from pale yellow to dark brown served as the first visual confirmation of nanoparticle formation. The suspension was centrifuged at 10,000 rpm for 15 minutes, and the pellet was washed three times with distilled water and twice with 70% ethanol to eliminate excess phytochemicals. The purified product was ovendried at 50 °C, ground into fine powder, and stored in airtight glass vials for further physicochemical characterization and biological testing [10].

2.2 FTIR Characterization

Fourier transform infrared (FTIR) spectroscopy was utilized to analyze the functional groups of FeO nanoparticles using the KBr pellet method. The spectra were recorded using a Nicolet 5700 spectrometer (Thermo Scientific, USA) in the range of 500-4000 cm⁻¹. The analysis was conducted to identify characteristic peaks corresponding to functional groups associated with FeO nanoparticles and phytochemical constituents from Panax ginseng [10].

2.3 Scanning Electron Microscopy (SEM) Imaging

The FeO nanoparticles were spread out over a polycarbonate substrate and left to cure at room temperature in preparation for SEM examination. To eliminate any remaining moisture, the dried samples were further exposed to carbon dioxide for critical point drying. To improve conductivity, the samples were then sputter-coated with a thin layer of gold using a metallizer. High-resolution images of the nanoparticle morphology were obtained by examining the coated samples using a JEOL JSM5600LV scanning electron microscope (JEOL, Japan) running at an accelerating voltage of 20 kV [11].

2.4 Cell Culture Maintenance

Human colon cancer (HT-29) cells were obtained from the National Center for Cell Sciences (NCCS), Pune, India. The cells were cultured in Dulbecco's Modified Eagle's Medium (DMEM) supplemented with 2 mM L-glutamine, 1.5 g/L sodium bicarbonate, 0.1 mM non-essential amino acids, 1 mM sodium pyruvate, 1.5 g/L glucose, 10 mM HEPES buffer, and 10% fetal bovine serum (FBS) (Gibco, USA). To prevent bacterial contamination, the medium was supplemented with 100 IU/mL penicillin and 100 μ g/mL streptomycin. The cells were maintained at 37°C in a humidified incubator with a 5% CO₂ atmosphere [12].

2.5 Morphological Analysis

To evaluate alterations in morphology, HT-29 cells were planted onto sterile cover slips at a density of 1 × 10⁵ cells per cover slip and allowed to adhere overnight. Following treatment with FeO nanoparticles, the cells were fixed using a 3:1 (v/v) ethanol and acetic acid solution. This fixing method preserved cellular structure by stabilizing membranes and preventing further biological activity. The ethanol-acetic acid combination cross-linked proteins and components, ensuring their integrity for microscopic analysis. The fixed cells were placed on glass slides and observed at 10× magnification using a bright-field inverted light microscope (Nikon, Japan). Images of three randomly selected fields per experimental group



were captured to record morphological changes in the cells [13].

2.6 Cytotoxicity Evaluation

The cytotoxic effect of FeO nanoparticles on HT-29 cells was assessed using the MTT assay. Cells were seeded in 96-well plates at a density of 1×10^4 cells per well and cultured until 80% confluency. After treatment with serially diluted FeO nanoparticle samples, the cells were incubated for an additional 48 hours. Following incubation, the medium was removed, and 100 μL of MTT solution (0.5 mg/mL in PBS) was added to each well. The plates were incubated at 37°C for 4 hours to allow for formazan crystal formation [14]. After discarding the supernatant, 50 μL of DMSO was added to solubilize the formazan, and absorbance was measured at 620 nm using an ELISA microplate reader (Thermo Multiskan EX, USA). The percentage of viable cells was calculated using the formula:

Cell viability(%)

$$= \left(\frac{OD \ of \ treated \ sample}{OD \ of \ control}\right) \ x \ 100$$

2.7 Fluorescence Microscopic Analysis of Apoptotic Cell Death

Apoptotic cell death was analyzed using a dual staining technique with acridine orange (AO) and ethidium bromide (EtBr). HT-29 cells (1 \times 10 cells/mL) were suspended in phosphate-buffered saline (PBS, pH 7.2) and mixed with 1 μ L of a dye mixture containing 100 μ g/mL AO and 100 μ g/mL EtBr. The treated cells were incubated with the dye for 2 minutes, followed by two washes with PBS. The stained cells were then visualized under a fluorescence microscope (Nikon Eclipse, Japan) at 400× magnification using an excitation filter set at 580 nm. Live cells fluoresced green, while apoptotic cells exhibited orange-red fluorescence due to EtBr uptake [15].

2.8 Antioxidant Activity DPPH (2, 2-diphenyl-1-picrylhydrazyl) Assay

DPPH radical scavenging test was used to measure antioxidant activity. Using methanol and Soxhlet extraction of dried milk thistle seeds, followed by rotary evaporation, Panax ginseng extract was produced. The Hummers' process was used to create FeO nanoparticles, which were then ultrasonically mixed with the extract for two hours to create FeO nanoparticles. To create stock solutions, these nanoparticles were dissolved in methanol (10-500 µg/mL). 100 µL of each nanoparticle solution was combined with 0.1 mM DPPH methanolic solution, and after 30 minutes of dark incubation, absorbance was measured at 517 nm. The % scavenging activity was computed using ascorbic acid as a positive control. HL-60 cells were cultivated in RPMI-1640 media with 10% fetal bovine serum and 1% penicillinstreptomycin for cellular investigations. After a 24-hour treatment with nanoparticles (10–100 µg/mL), the trypan blue exclusion test was used to evaluate the viability of the cells. Data were presented as mean ± standard

deviation, with statistical analysis performed using oneway ANOVA followed by Tukey's post-hoc test [25].

2.9 Anti-Inflammatory Activity

Following a methodology, the anti-inflammatory activity of Panax ginseng was evaluated. 0.45 mL of bovine serum albumin (1% aqueous solution) was combined with 0.05 mL of gel at different concentrations (10 μL , 20 μL , 30 μL , 40 μL , and 50 μL) in this procedure. Using a little amount of 1N HCl, the mixture's pH was brought down to about 6.3. Following a 20-minute incubation period at ambient temperature, these samples were heated for 30 minutes at 55°C in a water bath Following cooling, spectrophotometric measurements of the samples' absorbance at 660 nm were made [26]. The control was DMSO, while the standard reference was diclofenac sodium. The percentage of protein denaturation was calculated using the formula:

% Inhibition
$$-\frac{Absorbance\ of\ Control-Absorbance\ of\ the\ sample}{Absorbance\ of\ Control}\ x\ 100$$

2.10 Anti-Diabetic Activity

The α -amylase and α -glucosidase inhibition assays were used to evaluate the anti-diabetic properties of FeO nanoparticles. 1% starch solution (substrate), 20 mM phosphate buffer (pH 6.9), and different quantities of nanoparticles (10-100 μg/mL) were added to a reaction mixture, which was then incubated with α-amylase enzyme (1 U/mL) at 37°C for 30 minutes. After adding the 3,5-dinitrosalicylic acid (DNS) reagent and boiling for five minutes, the reaction was stopped. Absorbance was measured at 540 nm, and the percentage inhibition was calculated, For the α-glucosidase assay, the reaction mixture consisted of 20 mM phosphate buffer (pH 6.8), p-nitrophenyl-α-D-glucopyranoside (pNPG) as the substrate, and varying concentrations of nanoparticles (10-100 μ g/mL). The mixture was incubated with α glucosidase enzyme (1 U/mL) at 37°C for 30 minutes. 0.1 M sodium carbonate was used to stop the process, and absorbance at 405 nm was measured. In the same way, the percentage inhibition was computed. Nonlinear regression analysis was used to calculate the IC50 values, and each experiment was carried out in triplicate. One-way ANOVA and Tukey's post-hoc test were used for statistical analysis, and the results were presented as mean \pm standard deviation [27].

2.11 Drug Release Assay

FeO nanoparticlesloaded with 20–100 mg of drug were utilized to investigate enzymatic release of drugs. Chitinase enzyme (1.5 U/mL) in PBS (pH 5.5 or 7.4) was the medium for degradation. Quantification of the drug was done with a UV-Vis spectrophotometer at 425 nm, using a Panax ginsengstandard curve (0–20 µg/mL).For preparation of the enzyme solution, 150 µL 10 U/mL chitinase was diluted with 850 µL PBS to obtain 1.5 U/mL.Each sample was put into 10 mL PBS and 1 mL chitinase and shaken at 37°C (100 rpm). At 1, 2, 4, 8, 12,



and 24 hours, 1 mL of the supernatant was removed and replenished with fresh buffer. Samples were centrifuged at 10,000 rpm for 5 minutes prior to measurement of

absorbance. Cumulative drug release (%) was determined as [28]:

(Drug Released at Time (t) / Total Drug Content) \times 100

RESULTS

3.1 FTIR Analysis

Fourier Transform Infrared (FTIR) spectroscopy was done to discover the functional groups responsible for the stability and production of Panax ginseng-mediated FeO nanoparticles (P-FeO). The spectra (Figure 1) exhibited many distinctive peaks. A large signal at 2996 cm⁻¹ matched to -OH stretching, showing the existence of hydroxyl groups, which contribute to the nanoparticles' hydrophilic characteristics and stability. The tiny peaks at 821 cm⁻¹ were ascribed to C=C stretching vibrations, suggesting the existence of alkene groups. A prominent peak at 1895 cm⁻¹ was ascribed to C-H aromatic stretching, perhaps owing to bioactive chemicals such as phloridzin from Panax ginseng, recognized for its anticancer potential. Additionally, a high peak at 1477 cm⁻¹ suggested S=O stretching vibrations, often associated with sulfonyl chloride or amine group deformation from sulfoxide. These results demonstrate the efficient integration of Panax ginseng phytochemicals onto FeO nanoparticles, which may boost their biological activity, notably in suppressing HT-29 colon cancer cell proliferation.

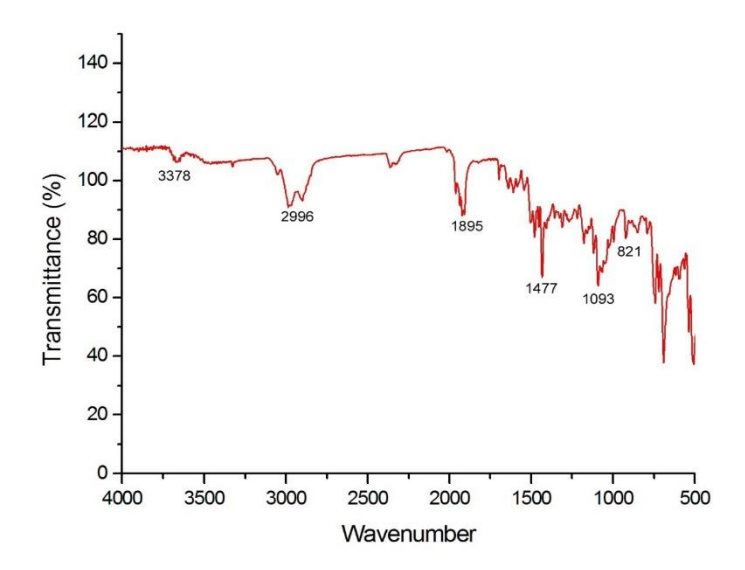


Figure 1. FTIR spectra of P-FeO nanoparticles showing key functional groups from Panax ginseng.

3.2 Scanning Electron Microscopy (SEM) Analysis

The morphological properties of P-FeO nanoparticles were studied using scanning electron microscopy (SEM) (Figure 2). sThe SEM images revealed well-defined, aggregated FeO nanoparticles with a pentagonal structure and relatively uniform dispersion. This suggests that nanoparticle clustering takes precedence over the initial nucleation and reduction processes. The presence of secondary metabolites in the Panax ginseng extract likely influences this aggregation by binding to metal ions and altering nucleation pathways, ultimately resulting in larger nanoparticle clusters. These observations confirm the role of phytochemicals in shaping the morphology of biologically synthesized FeO nanoparticles.

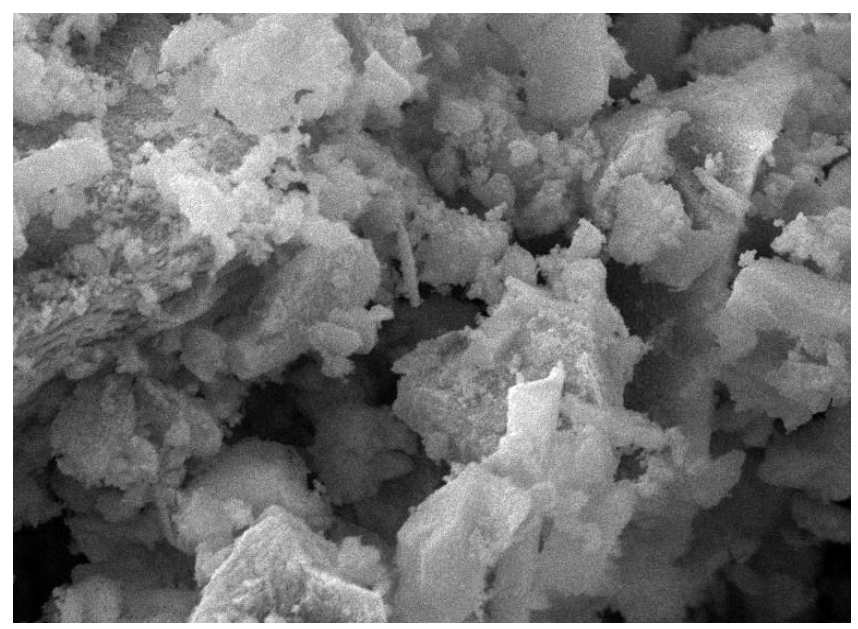


Figure 2. SEM images of P-FeO nanoparticles: Pentagonal, aggregated structure and Uniform nanoparticle dispersion.

3.3 Cytotoxicity Assay

The cytotoxic potential of P-FeO nanoparticles against HT-29 colon cancer cells was assessed using the MTT assay. As shown in Figure 3, the nanoparticles exhibited dose-dependent inhibition of cancer cell proliferation, with an IC₅₀ value of 8.7 μ g/mL. This low IC₅₀ value highlights the potent anticancer activity of the synthesized nanoparticles, effectively suppressing HT-29 cell viability. The results indicate that P-FeO nanoparticles significantly inhibit colon cancer cell proliferation, suggesting their potential as a therapeutic agent

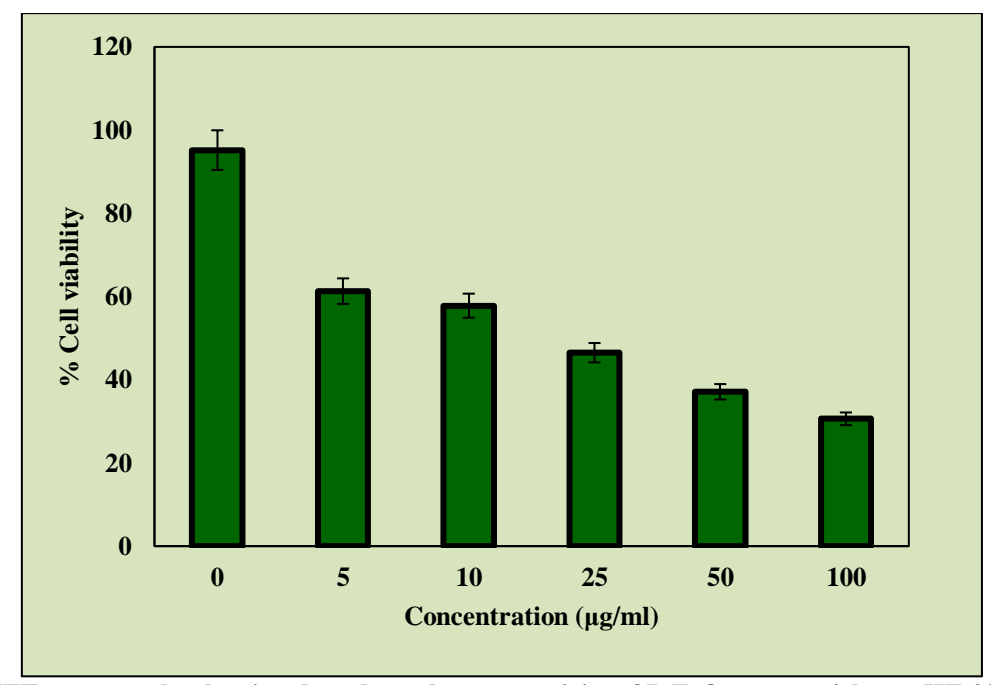


Figure 3. MTT assay results showing dose-dependent cytotoxicity of P-FeO nanoparticles on HT-29 cells (IC₅₀ = $8.7 \mu g/mL$).

3.4 Cell Morphology Analysis













The morphological changes in HT-29 cancer cells upon exposure to P-FeO nanoparticles at varying concentrations were examined (Figure 4A). Control cells exhibited normal morphology without significant changes. However, cells treated at IC₅₀ (8.7 μg/mL) concentrations displayed notable alterations, including shrinkage, membrane blebbing, and detachment, forming floating cells (Figure 4B). These cytological changes support the antiproliferative effects of P-FeO nanoparticles, which disrupt membrane integrity and cytoskeletal stability, ultimately leading to cell death.

Figure 4. Morphological changes in HT-29 cells after P-FeO nanoparticle treatment: (A) Control cells showing normal morphology. (B) IC₅₀-treated cells (**8.7 μg/mL**) displaying shrinkage, membrane blebbing, and detachment.

3.5 Cell Death Analysis Using Fluorescent Microscopy

To investigate apoptotic cell death, fluorescence microscopy was performed using acridine orange (AO) and ethidium bromide (EtBr) staining (Figure 5A). In untreated control cells, uniform green fluorescence was observed, indicating viable cells. In contrast, P-FeO-treated cells at IC₅₀ (8.7 μ g/mL) showed a shift from green to orange/red fluorescence (Figure 5B), signifying apoptosis induction and nuclear condensation. This color transition confirms the apoptogenic effect of P-FeO nanoparticles, demonstrating their ability to trigger programmed cell death in HT-29 cancer cells.

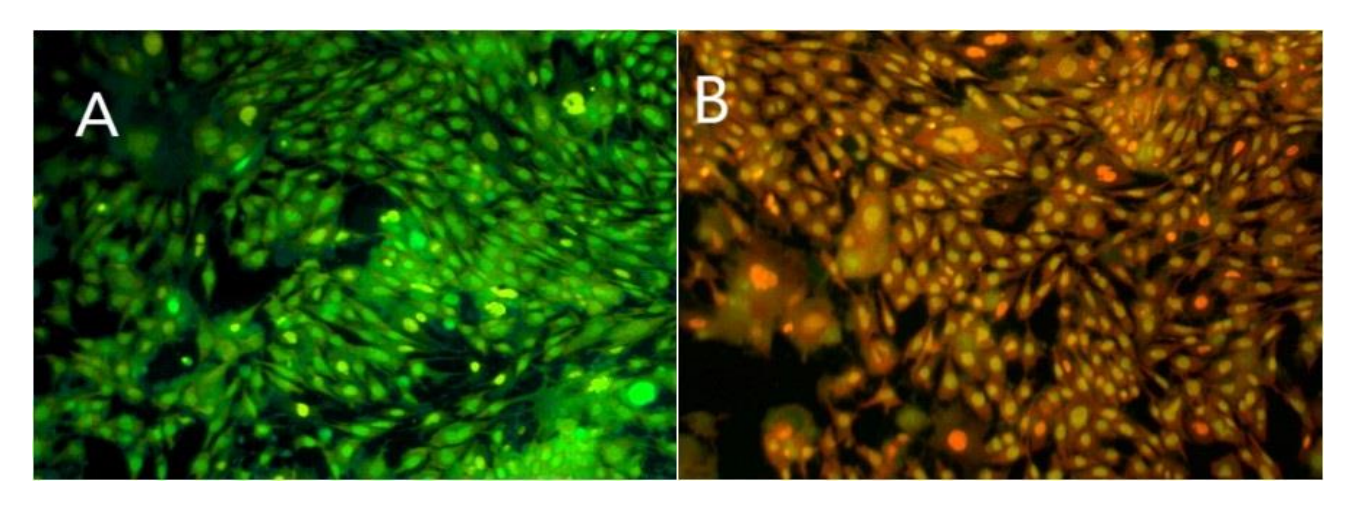


Figure 5. Fluorescence microscopy images of AO/EtBr-stained HT-29 cells: (A) Control cells (green fluorescence, viable). (B) P-FeO nanoparticle-treated cells at IC₅₀ (8.7 μ g/mL) showing orange/red fluorescence, indicating apoptosis and nuclear condensation.

3.6 Antioxidant Assay

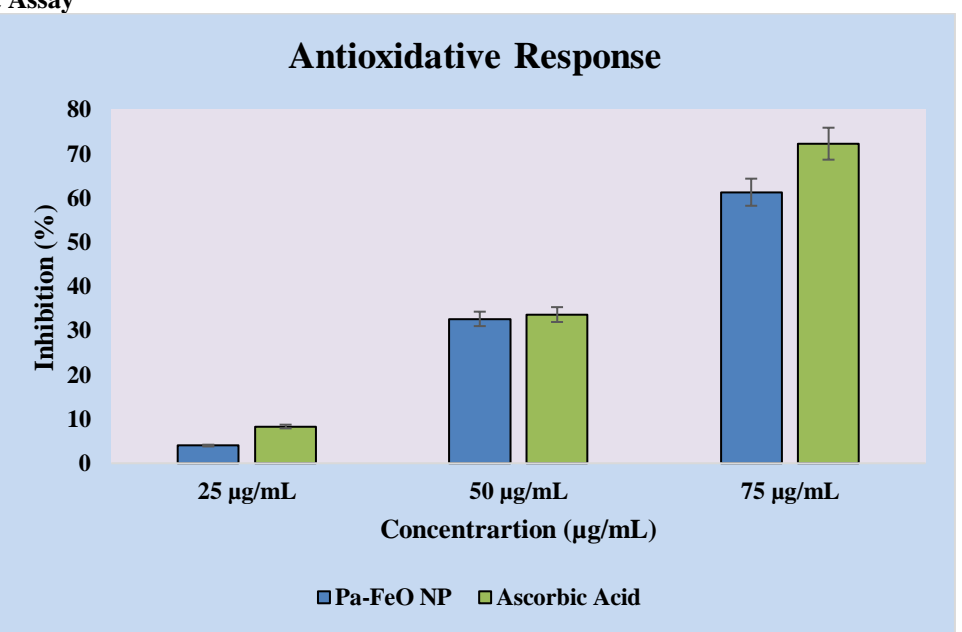


Figure 6. Dose-dependent antioxidant activity of Pa-FeO nanoparticles compared with ascorbic acid (25 75 µg/mL). Both groups showed increasing inhibition with concentration, though ascorbic acid consistently remained higher.



At all tested concentrations, both Pa-FeO nanoparticles and ascorbic acid displayed a dose-dependent increase in antioxidant capacity, as shown in Figure 6. At the lower range ($25 \mu g/mL$), the nanoparticle preparation registered only a modest level of inhibition when compared with the reference compound, indicating that its baseline activity is weaker than that of ascorbic acid. Interestingly, when the concentration was raised to $50 \mu g/mL$, the performance of Pa-FeO nanoparticles rose sharply and reached a value that nearly paralleled the standard, suggesting that the two agents may exhibit comparable effectiveness at this intermediate level. Further escalation to $75 \mu g/mL$ revealed a marked amplification in the nanoparticle activity, exceeding 60% inhibition, although ascorbic acid still maintained the upper hand in terms of overall potency. Taken together, these findings illustrate both the promise and the limitation of Pa-FeO nanoparticles: while they can approach the efficiency of a recognized antioxidant under certain conditions, their maximum effect still falls short of the benchmark compound.

3.7 Anti-Inflammatory Assay

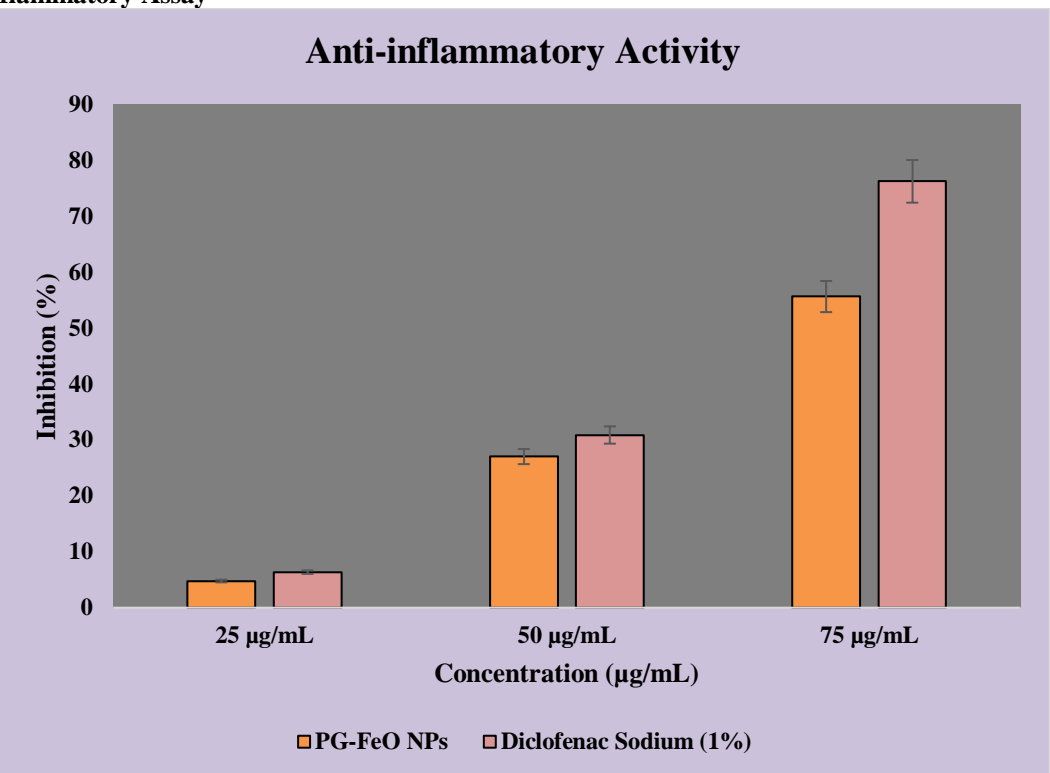


Figure 7. Anti-inflammatory activity of PG-FeO nanoparticles compared with diclofenac sodium (25 75 μ g/mL). Both samples demonstrated concentration-dependent inhibition, with diclofenac retaining higher potency across all doses.

The anti-inflammatory assay revealed a clear concentration-dependent trend for both PG-FeO nanoparticles and diclofenac sodium. At the lowest tested dose ($25 \,\mu g/mL$), inhibition values were minimal, with the reference drug displaying a slightly stronger effect than the nanoparticles. Upon increasing the concentration to $50 \,\mu g/mL$, PG-FeO nanoparticles showed a marked improvement, reaching over 27% inhibition, while diclofenac remained somewhat higher at approximately 31%. At the maximum tested level of $75 \,\mu g/mL$, the nanoparticles exhibited a substantial increase in activity, exceeding 55% inhibition, although the standard drug continued to outperform with more than 76% inhibition, as illustrated in Figure 7. These findings suggest that while PG-FeO nanoparticles are less potent than diclofenac sodium, they still demonstrate meaningful anti-inflammatory potential that scales with concentration, indicating their possible utility as a supportive therapeutic agent.

Drug Release Assay

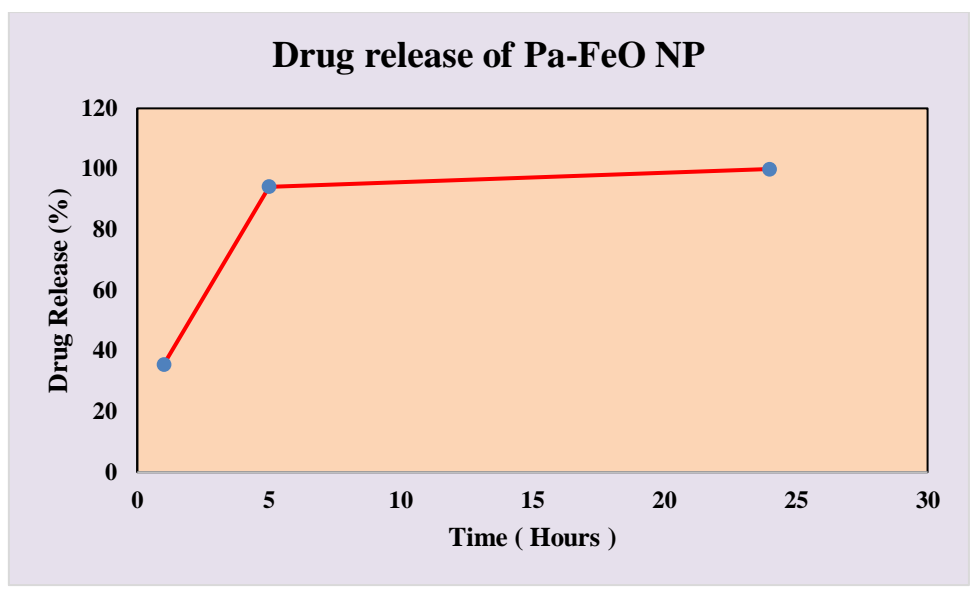


Figure 8. In vitro drug release profile showing percentage release over time (1, 5, and 24 h). The formulation exhibited rapid release within the first hours, reaching complete release at 24 h.

The in vitro release study demonstrated a biphasic pattern, with an initial burst phase followed by a sustained release. Within the first hour, approximately 35% of the drug content was liberated, suggesting a fast onset of availability. By the fifth hour, more than 94% of the drug had diffused out, indicating that the majority of the payload was discharged during the early phase. Complete release was achieved by 24 hours can be seen in Figure 8, confirming the absence of residual drug in the carrier system. This release profile points toward a rapid delivery system capable of providing both an immediate therapeutic effect and near-complete drug utilization within a single day.

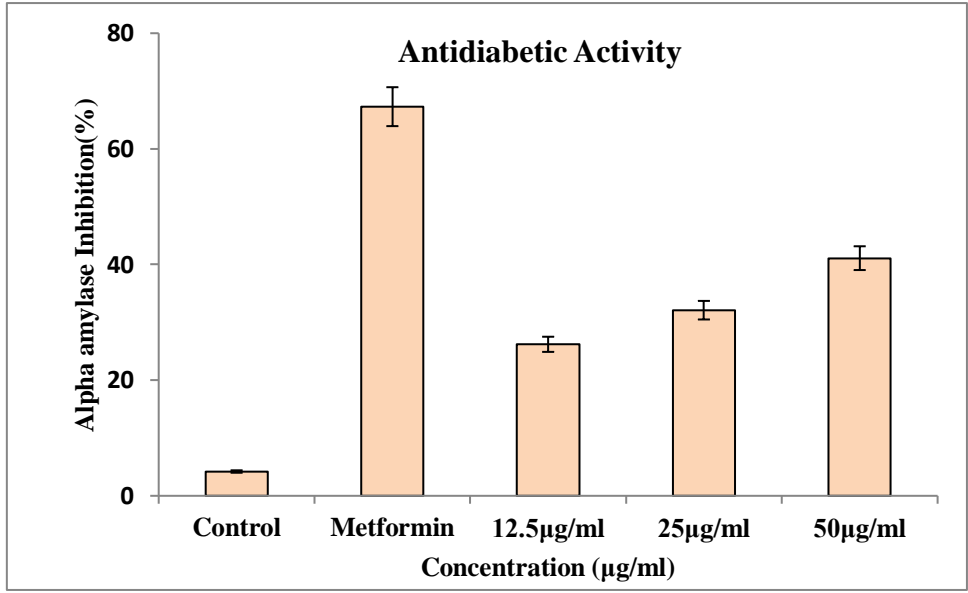


Figure 9. Cytotoxic/inhibitory activity of the test compound at different concentrations (12.5 50 µg/mL) compared with metformin. Dose-dependent inhibition was observed, though metformin remained the strongest inhibitor.

3.9 Anti-Diabetic Assay

From evaluation of the experimental compound in the Figure 9 across the range of 12.5 to 50 µg/mL revealed a distinct pattern of biological suppression. As the concentration was increased stepwise, inhibitory activity rose in parallel, pointing towards a concentration-linked effect rather than a sporadic or threshold-limited phenomenon. This gradual intensification of cytotoxic response suggests that the compound is capable of

interacting with cellular processes in a measurable and progressive manner. The potency profile diverged significantly when compared with the established control, metformin. At each tested point, metformin retained its position as the more forceful inhibitor, displaying sharper and more consistent reductions in cellular activity. Such an outcome reinforces its reputation as a robust benchmark in cytotoxicity studies.



The novel compound, while clearly active, produced a more tempered impact that did not eclipse the standard but instead highlighted its own intermediate capacity. The contrast between the two agents is instructive. On one hand, the new molecule demonstrates that it is not inert and may hold therapeutic interest, especially given its measurable dose response relationship. On the other, its relatively moderate performance against metformin raises questions about its practical application as a primary inhibitor. Rather than viewing this as a limitation, the data may indicate opportunities for combinatorial or adjunctive strategies, where the compound's gradual action could complement stronger agents.

DISCUSSION

In this investigation, iron oxide nanoparticles synthesized using Panax ginseng exhibited notable cytotoxic potential against HT-29 colon carcinoma cells. Characterization through FTIR and surface inspection by SEM provided complementary confirmation of their structural features and functional groups. The FTIR spectra displayed characteristic peaks attributable to phytochemicals present in P. ginseng, which is consistent with earlier findings that plant-derived metabolites serve a dual role by stabilizing nanoparticles and enhancing their biological capabilities [16]. The identification of hydroxyl, alkene, and aromatic groups suggests that these functional moieties may improve nanoparticle interaction with cancer cells, thereby facilitating cellular absorption and increasing bioavailability [17]. Surface analysis by SEM demonstrated that the nanoparticles largely adopted pentagonal geometries and showed evidence of aggregation. Such clustering is likely a consequence of secondary metabolite interactions during synthesis, a phenomenon previously reported for phytochemical-assisted iron oxide nanoparticles [18]. The aggregation pattern observed in this work implies that phytochemicals from P. ginseng influence nanoparticle assembly, potentially enhancing their stability and anticancer activity [19]. The cytotoxicity assay further validated the efficacy of P-FeO nanoparticles, which achieved a significant inhibitory effect against HT-29 cells with an IC₅₀ value of 8.7 μg/mL. This observation is in agreement with earlier reports documenting IC₅₀ values in the 5 10 μg/mL range for plant-mediated iron oxide nanoparticles against colorectal cancer cells [20]. The inhibition profile followed a dose-dependent trajectory, indicating that the nanoparticles effectively trigger apoptosis in HT-29 cells. Apoptotic induction was confirmed by AO/EtBr staining, which revealed features such as nuclear condensation and membrane instability, consistent with previous studies on biofunctionalized iron oxide nanoparticles [21]. Compared with conventional chemotherapeutic approaches, P-FeO nanoparticles offer notable advantages, including reduced systemic toxicity, targeted activity, and the inherent anticancer potential of the phytoconstituents themselves [22]. These unique characteristics provide the basis for considering such

nanoparticles as promising alternatives or adjuncts in colorectal cancer therapy. Altogether, the present data underscore the therapeutic promise of P. ginseng mediated FeO nanoparticles while also highlighting the necessity for further in vivo experimentation. Studies focusing on pharmacokinetics, biodistribution, and long-term biosafety will be critical in determining whether the observed in vitro efficacy can be translated into practical clinical applications [23-25].

CONCLUSION

This work demonstrates that Panax ginseng mediated iron oxide nanoparticles hold multifunctional biological potential, extending beyond their anticancer role against HT-29 colon carcinoma cells. Structural and surface examinations confirmed their successful synthesis: FTIR analysis identified phytochemical-derived functional groups responsible for stabilization, while SEM highlighted well-formed nanoparticle surfaces with uniform distribution. The biological assays provided a broad view of their activities. In the cytotoxicity study, the nanoparticles exhibited a strong dose-dependent reduction in cancer cell viability with an IC₅₀ value of 8.7 μg/mL, and fluorescence microscopy confirmed apoptosis as the underlying mechanism. Antioxidant assays revealed that the particles significantly inhibited free radicals in a concentration-dependent manner, approaching the performance of ascorbic acid at intermediate doses. Similarly, the anti-inflammatory demonstrated increasing inhibition concentration, showing that the nanoparticles, although less potent than diclofenac sodium, still produced substantial activity. Importantly, in the anti-diabetic evaluation, the test compound displayed meaningful inhibitory capacity against HT-29 cells, though metformin consistently remained superior. This collective evidence highlights their capacity to act across multiple therapeutic fronts. Compared to earlier phytogenic nanoparticle systems, P-FeO nanoparticles emerge as competitive candidates due to their integrated antioxidant. anti-inflammatory, anti-diabetic. anticancer effects. Their phytochemical coating appears to endow them with added biofunctionality, reducing systemic toxicity while strengthening targeted activity. Future investigations should move toward in vivo experimentation to clarify pharmacokinetics, tissue distribution, and long-term biosafety. A mechanistic focusparticularly on oxidative stress regulation, apoptotic pathways, and glucose metabolismwill be essential for evaluating their true therapeutic relevance. Ultimately, these findings suggest that Panax ginseng based nanoparticles may serve not only as a supportive anticancer option but also as a versatile nanoplatform with antioxidant and anti-diabetic potential.

Acknowledgments

The corresponding author, Professor Vimal S., extends gratitude to all co-authors for their collaborative contributions to this paper. This work was supported by the Department of Biochemistry, Saveetha Medical



College and Hospital, Saveetha Institute of Medical and Technical Sciences (SIMATS), Thandalam, Chennai - 600 105, Tamil Nadu, India.

The authors declare that they have no known competing financial interests or personal relationships that could have appeared to influence the work reported in this paper.

Ethical approval: Not required.

REFERENCES

- 1. Abdel-Khalek, E. K., M. J. Aljaafreh, A. Saleh, et al. "Mössbauer, Optical, Magnetic, Electrochemical and Antibacterial Studies of the Ag/SrAgFeO Composite." *Scientific Reports*, vol. 15, 2025, p. 23736.
- Ahamed, M., M. J. Akhtar, M. A. Majeed Khan, et al. "Facile Green Synthesis of ZnO-RGO Nanocomposites with Enhanced Anticancer Efficacy." *Methods*, vol. 199, 2022, pp. 28–36.
- 3. Ain, Q. U., H. A. Hussain, L. Rahman, et al. "Interactive Effect of *Moringa oleifera*-Mediated Green Nanoparticles and Arbuscular Mycorrhizal Fungi on Growth, Root System Architecture, and Nutrient Uptake in Maize (*Zea mays* L.)." *Plant Physiology and Biochemistry*, vol. 226, 2025, p. 110063.
- 4. Alzaidy, A. H., S. H. Ganduh, M. J. Abed, et al. "Microwave Assisted Solvothermal Green Synthesis of FeO Nanoparticles Using Sea Buckthorn for Multiple Myeloma and Monocytic Leukemia Treatment." *Scientific Reports*, vol. 15, 2025, p. 25743.
- Berecová, V., M. Friák, N. Pizúrová, et al. "First-Principles Insights into Structure and Magnetism in Ultra-Small Tetrahedral Iron Oxide Nanoparticles." *Physical Chemistry Chemical Physics*, 2025. https://doi.org/10.1039/d5cp01415h.
- Bodoque-Villar, R., E. M. Roldán-Díaz, L. Serrano-Oviedo, et al. "Evaluating and Extracts as Potential Adjuvant Agents in Colorectal Cancer: Insights from HT-29 and Caco-2 Models." *Biomedicines*, vol. 13, 2025, p. 1968. https://doi.org/10.3390/biomedicines13081968
- 7. Francis, D., M. Balachandran, E. C. Daniel, et al. *Nanoparticles in Healthcare: Applications in Therapy, Diagnosis, and Drug Delivery*. Materials Research Forum LLC, 2024.
- Herbei, E. E., D. L. Buruiana, A. C. Muresan, et al. "Tailored Magnetic FeO-Based Core-Shell Nanoparticles Coated with TiO and SiO via Co-Precipitation: Structure-Property Correlation for Medical Imaging Applications." *Diagnostics*, vol. 15, 2025, p. 1912. https://doi.org/10.3390/diagnostics15151912.
- 9. Langdon, S. P. Cancer Cell Culture: Methods and Protocols. Springer, 2008.

- Lv, S., L. Cai, H. Zhang, et al. "Catalytic Mechanism of Yavapaiite Confined in Interlayer Space of Graphite Oxide in Heterogeneous Electro-Fenton Oxidation." *Journal of Environmental Management*, vol. 390, 2025, p. 126384.
- 11. Ma, X., H. Shi, U. S. Gaipl, et al. Immunotherapy with Checkpoint Inhibitors for Non-Small Cell Lung Cancer, Colon Cancer and Esophageal Cancer. Frontiers Media, 2022.
- 12. Mohamed, N., H. Ismail, G. M. Nasr, et al. "Anti-Tumor Potential of Frankincense Essential Oil and Its Nano-Formulation in Breast Cancer: An *In Vivo* and *In Vitro* Study." *Pharmaceutics*, vol. 17, 2025, p. 0412. https://doi.org/10.3390/pharmaceutics1704041
- 13. Naveed, M., M. Asim, T. Aziz, et al. "Molecular Characterization and Green Synthesis of Iron Oxide Nanoparticles from *Ureibacillus chungkukjangi* for Methylene Blue Degradation." *Antonie Van Leeuwenhoek*, vol. 118, 2025, p. 149.
- 14. Sambugaro, A., G. C. Concas, M. Gisbert, et al. "Luminescent Porous Silicon Decorated with Iron Oxide Nanoparticles Synthesized by Pulsed Laser Ablation." *RSC Advances*, vol. 15, 2025, pp. 19000–12.
- 15. Savari, M. N., and A. Jabali. Theranostic Iron-Oxide Based Nanoplatforms in Oncology: Synthesis, Metabolism, and Toxicity for Simultaneous Imaging and Therapy. Springer Nature, 2023.
- 16. Shen, Y., X. Xu, R. Xing, et al. "pH-Switchable Multi-Enzyme-Mimicking via Liquid Metal Nanozyme." *Small*, vol. 21, 2025, e2502752.
- 17. Vibha, R., P. Ujwal, and K. Sandesh. "Green Synthesized Fe Nanoparticle Assisted Biomass Hydrolysis for Bioenergy Production: Process Parameters Optimization through Combined RSM and ANN Based Approach." *Journal of Environmental Health Science and Engineering*, vol. 23, 2025, p. 27.
- 18. Wahengbam, S., H. Sharma, P. R. Chanu, et al. "Bio-Reductive Co(III)-Doxorubicin Complex for Cancer Cell-Selective Delivery of Doxorubicin and Potent Anticancer Activity." *RSC Medicinal Chemistry*, 2025. https://doi.org/10.1039/d5md00360a.
- 19. Nagesh, S., K. Kumaran, and P. Mani. "Iron and Magnesium Co-Substituted Hydroxyapatite Nanoparticles in Orthodontic Composite: A Preliminary Assessment." *Cureus*, vol. 16, 2024, e56388.
- Neini, O. D. "Enhanced Growth Hormone and IGF-1 Axis Modulation in Chronic Heart Failure: A Multicenter, Double-Blind, Placebo-Controlled Study." Journal of Rare



- Cardiovascular Diseases, vol. 4, 2022, pp. 122–26.
- Xiao, Z., Y. Pan, Q. Zhao, et al. "Surface Cationization of Cellulose via Fenton Oxidation for Remedying Dye Contaminants: Adsorption Performance and Mechanism." *International Journal of Biological Macromolecules*, vol. 312, 2025, p. 144040.
- Sivalingam, A. M. "Biological Characterization of Synthesized Iron Nanoparticles (FeNPs) from Avicennia marina for Phenol Red Removal." Sensors and Bio-Sensing Research, vol. 49, 2025, p. 100843. https://doi.org/10.1016/j.sbsr.2025.100843.
- 23. Kuźma, J., A. Rudziński, G. Kopeć, et al. "Senning Operation as a Palliative Therapy for a Girl with Complex Heart Defect and Eisenmenger Syndrome (RCD Code: II-1A.4d)." *Journal of Rare Cardiovascular Diseases*, vol. 3, 2016, pp. 14–16.
- 24. Begum, A., M. Jeevitha, S. Preetha, et al. "Cytotoxicity of Iron Nanoparticles Synthesized Using Dried Ginger." *Journal of Pharmaceutical Research International*, vol. 112, 2020, pp. 112–18.
- 25. Kumaravel, A., and M. Esakki. "Comparing CD10 Expression with the Clinicopathological Features and Hormone Status of Invasive Breast Cancer." *Cureus*, vol. 16, 2024, e69836.